CHEMELECTROCHEM

Supporting Information

Electroless Nanoplating of Pd–Pt Alloy Nanotube Networks: Catalysts with Full Compositional Control for the Methanol Oxidation Reaction

Tobias Stohr,* Angelina Fischer, Dr. Falk Muench, Markus Antoni, Stephan Wollstadt, Christian Lohaus, Ulrike Kunz, Prof. Dr. Oliver Clemens, Prof. Dr. Andreas Klein, and Prof. Dr. Wolfgang Ensinger

1.1. EDX

The following extract shows an example EDX-measurement (fig. 1) that was conducted in-situ during SEM analysis. Atomic Pd/Pt-ratios were calculated by the standard ZAF-correction method. For each of the presented samples, the corresponding atomic Pd/Pt-amounts were calculated by the average of five random measurement points on the sample, with 50s-long measurements. Fig.1 shows an example EDX-spectrum on $Pd_{65}Pt_{35}$-NTs. The expected errors of measured atomic amounts are in the range of a few percent: Typically, the as-synthesized NTs underlie a natural distribution of metal concentrations with a standard deviation below 1% and additionally, the measurement in the present setup and measurement time is accurate with a standard deviation typically below 2%. Table 2 gives insight into the calculation of average atomic percentages for Pd and Pt with respect to the entire sample size of the seven NTNW-samples with different PdPt-composition.

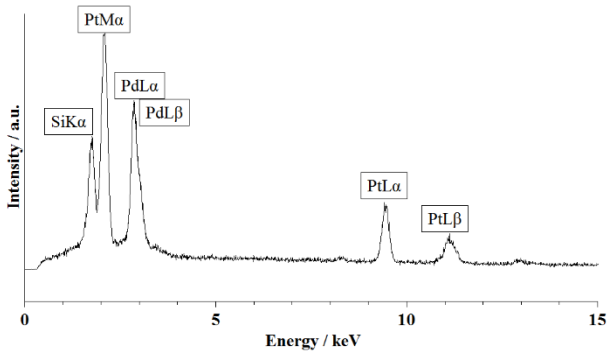

Fig. 1: Example EDX-spectrum on $Pd_{65}Pt_{35}$-NTs

Table 1: Example EDX-measurement data of $Pd_{65}Pt_{35}$-NTs, from left to right: Element line, weight-percentage, atomic percentage, K-ratio (intensity ratio to internal standard), corrections for the atomic number Z, the absorption A and fluorescence F.

Element	Wt%	At%	K-Ratio	Z	A	F
Pd-L	50.93	65.56	0.2965	1.0380	0.5608	1.0000
Pt-L	49.07	34.44	0.4661	0.9480	1.0020	1.0000
Total	100.0	100.0				

Table 2: All EDX-measurement points with respective Pd(at%) and Pt(at%) for all seven investigated NTNW-samples. Five measurement points were analyzed for each sample (1-5) and the average (Avg) was calculated.

Point	1		2		3		4		5		Avg	Avg
	Pd at%	Pt at%	Pd at%	Pt at%	Pd at%	Pt at%	Pd at%	Pt at%	Pd at%	Pt at%	Pd at%	Pt at%
$Pd_{100}Pt_{0}$	100.0	0.0	100.0	0.0	100	0.0	100.0	0.0	100.0	0.0	100.0	0.0
$Pd_{80}Pt_{20}$	80.5	19.5	79.7	20.3	78.8	21.2	80.3	19.7	81.2	18.8	80.1	19.9
$Pd_{75}Pt_{25}$	73.9	26.1	76.3	23.7	75.1	24.9	75.6	24.4	74.5	25.5	75.08	24.92
$Pd_{50}Pt_{50}$	49.8	50.2	51.1	48.9	50.6	49.4	50.4	49.6	48.8	51.2	50.14	49.86
$Pd_{30}Pt_{70}$	29.9	70.1	30.2	69.8	31.4	68.6	29.1	70.9	30.0	70.0	30.12	69.88
$Pd_{20}Pt_{80}$	21.0	79.0	20.3	79.7	20.7	79.3	19.6	80.4	18.9	81.1	20.1	79.9
$Pd_{0}Pt_{100}$	0.0	100.0	0.0	100.0	0.0	100.0	0.0	100.0	0.0	100.0	0.0	100.0

1.2. XRD

In the following, the X-ray diffractograms of the three analyzed samples Pd-NTs, Pt-NTs and $Pd_{50}Pt_{50}$-NTs are shown (fig. 2-4). Reference values for the respective reflexes and their corresponding intensity ratios were extracted from corresponding pdf-files.[58,59]

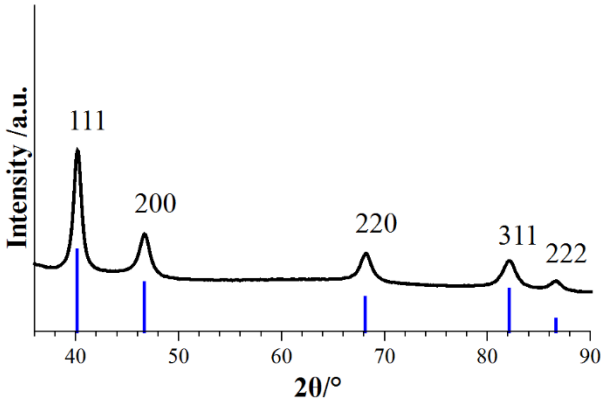

Fig.2: X-ray diffractogram of the monometallic Pd-NTs

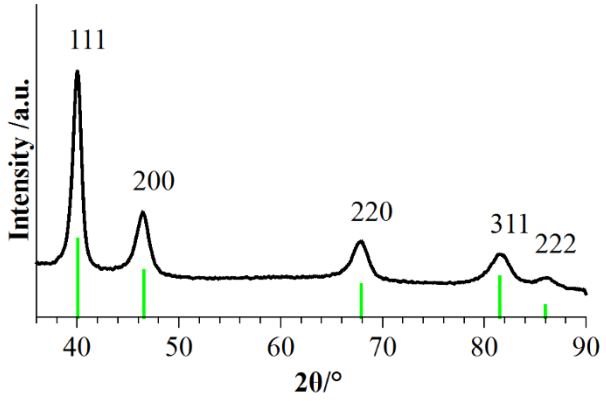

Fig. 3: X-ray diffractogram of the monometallic Pt-NTs

The diffraction patterns of the monometallic system-confining samples (fig.2 and 3) show indeed that they consist of pure Pd and Pt. The diffraction data is in good agreement with reference data from respective bulk metal samples (green reflex lines for Pd and blue for Pt, respectively). As a result of the lanthanide contraction which leads to equal atom sizes of Pd and Pt and the fact, that both transition metals crystallize in a fcc-structure under standard

conditions, both monometallic NT diffraction patterns equal each other and only differ slightly at higher 2θ-values. For Pt, characteristic reflexes of its diffraction pattern are found at lower values, because of its slightly bigger lattice parameter.[58,59]

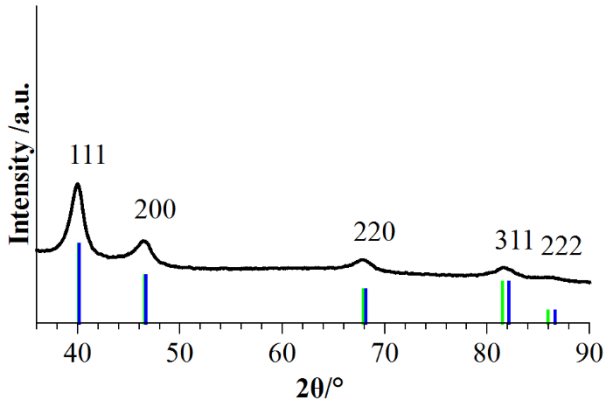

Fig. 4: X-ray diffractogram of the bimetallic $Pd_{50}Pt_{50}$-NTs

The $Pd_{50}Pt_{50}$-NT's show similar diffraction behavior, indicating that they consist of a mixture of bimetallic, Pd/Pt-alloy nanoparticles of different Pd/Pt-composition. A magnification of the (220)-reflex for all three samples underlines the asymmetry of the $Pd_{50}Pt_{50}$-NT's reflex and its broadening (fig. 4), especially to lower 2θ-values, in comparison to the monometallic NT's. Though this is not a clear evidence for alloy formation, the XRD patterns show indices that neither the $Pd_{50}Pt_{50}$-NT's consist of pure Pd- and Pt-phases, which would result in two separate reflexes, nor is there only one specific alloy phase present, which would lead to one distinct and symmetrical reflex. However, the $Pd_{50}Pt_{50}$-NT's grains seem partially dominated by the bigger lattice parameter of Pt, leading to a reflex-broadening to lower 2θ-values for the (220)-reflexes. Vegard's law was applied for the underlying Pd/Pt-system, since both metals have similar atom sizes and crystallize in the fcc-structure. From Vegard's law it can be calculated the expected angle at which the $Pd_{50}Pt_{50}$-NT's (220)-reflex should theoretically appear:

With a_{Pd}=389.019 pm, a_{Pt}=391.61 pm as the lattice parameters for Pd and Pt respectively,[58,59] Vegard's equation can be simplified for the $Pd_{50}Pt_{50}$-sample as it follows:

$$a_{PdPt} = a_{Pd}(1-x) + a_{Pt}\,x = 0.5(a_{Pd} + a_{Pt})$$

$$= 390.3145\,pm$$

The Bragg-equation for a cubic system can be written as:

$$\sin(\theta)^2 = \frac{\lambda^2}{4a_{PdPt}} \times (h^2 + k^2 + l^2), \qquad \text{(eq.1)}$$

With

λ = 154.12 ± 0.04 pm; "*wavelength of the Cu-Kα-line*"

a_{PdPt} = 390.3145 pm; "*alloy lattice parameter calculated by Vegard's equation*"

By transforming the Bragg-equation for cubic systems (eq.10) the theoretically expected 2θ-value for the 220-reflex of an ideal $Pd_{50}Pt_{50}$-alloy can be calculated:

$$2\theta_{220} = 2\sin^{-1}\left(\sqrt{\frac{2\times\lambda^2}{{a_{PdPt}}^2}}\right) = 67.893 \pm 0.03° \qquad \text{(eq.2)}$$

The experimentally found $2\theta_{220}$- value for the $Pd_{50}Pt_{50}$-NTs is 67,9015°. This value is in good agreement with our theoretical calculations, though it does not take into account every aspect that could cause a deviation of the alloy lattice parameter from Vegard's law: For example, the interaction of Pd and Pt atoms in the solid is neglected in Vegard's law by its definition and furthermore, since we compare the theoretical value with the one of NTNWs, there is an extraordinary amount of surface sites and grain boundaries, which have an influence on the forming crystalline structures and therefore on the lattice parameter. Both theoretical confinements resulting from the calculated $2\theta_{220}$-reflex at $2\theta = 67.893 \pm 0.03°$ are shown in the magnification of the overlaid diffractograms in fig. 5.

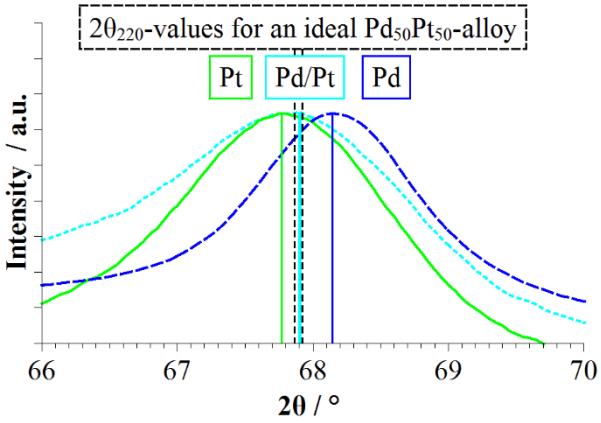

Fig. 5: X-ray diffractogram of the 220-reflex of all three investigated samples: Pd-NTs (dark blue line), $Pd_{50}Pt_{50}$-NTs (cyan line) and Pt-NTs (green line).

Similar to the calculations above regarding the lattice parameter, the Rietveld-refinement included in the main paper (see 3.4.) gives a much more reliable and detailed result with respect to structural and phase characteristics.

1.3. TEM

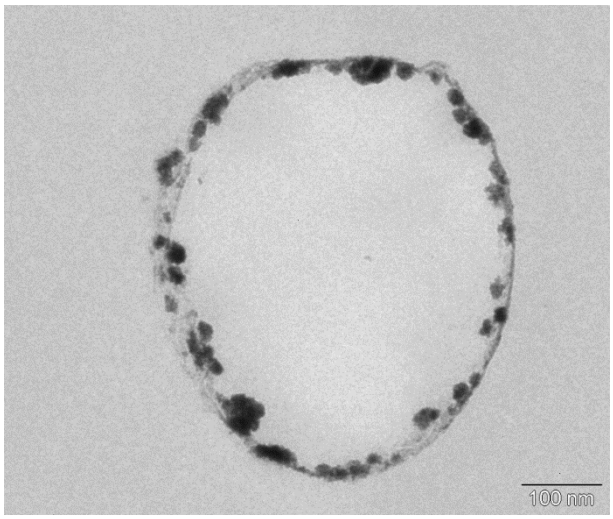

Fig. 6: TEM-picture of a PdPt-NT in the early growth stage.

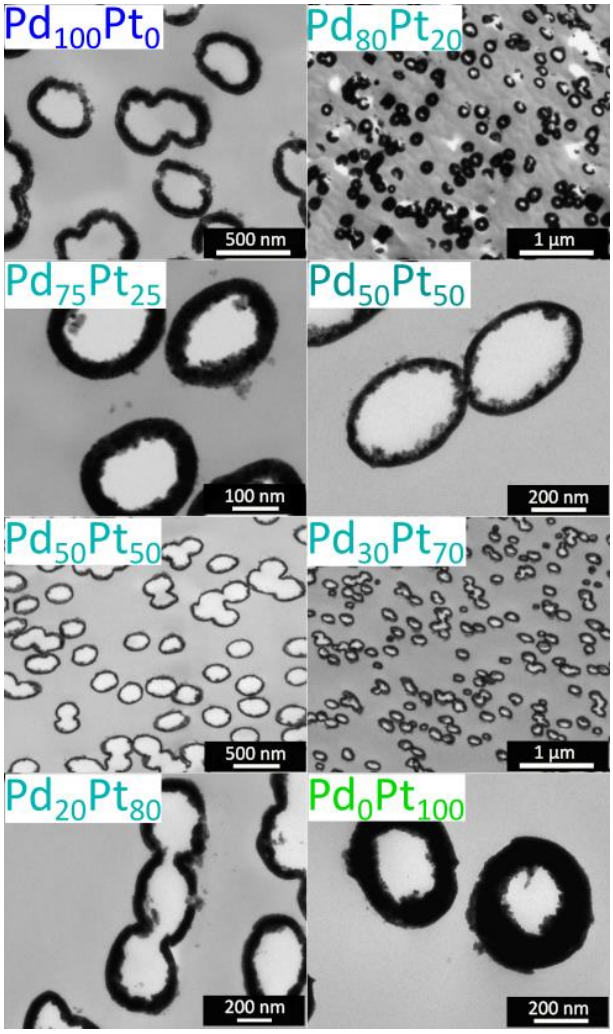

Fig. 7: TEM-pictures of PdPt-NT samples with specified Pd/Pt-at% ratio

To further underline the aspects of the first growth stage during electroless plating, the 2D-growth onto the nano channel wall, the Pd/Pt-NTNW was investigated before completing its plating procedure (fig.6). The TEM depicts islands up to 50 nm in diameter that attached to the nanochannels surface. In this early stage of the electroless plating, the metallic particle islands are not already fully coherent. With oncoming particles out of the plating solution, the empty spaces are filled up by the growth of surrounding islands and further nucleation processes. The following fig. 7 shows the TEM-analysis of the seven Pd/Pt-archetypes presented in our work.

1.4. CV

Table 3: Conditions for all conducted CV-experiments. Electrolytes, scan rates and reference electrodes.

	ESCA	MOR	CO-stripping	longterm cycling
Electrolyte	0.5 M H_2SO_4	0.5 M H_2SO_4 + 1.2 M methanol	0.5 M H_2SO_4	0.5 M H_2SO_4
Scan rate	50 mV/s	50 mV/s	10 mV/s	150 mV/s
Ref. electrode	$Hg\|Hg_2SO_4$	$Hg\|Hg_2SO_4$	Ag|AgCl	Ag|AgCl

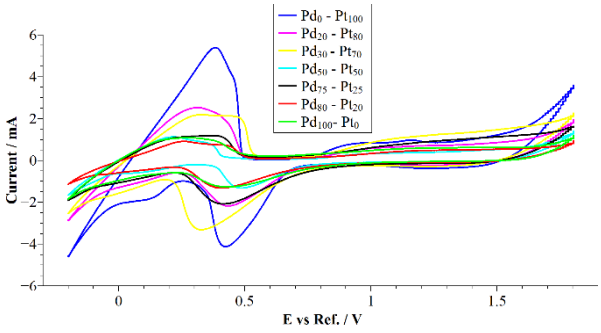

Fig.8: CVs for the ECSA determination of all seven investigated NTNW-samples

The ESCAs A_H were determined by integrating the oxidation peak of H-desorption currents subtracting the capacitive currents from the following bilayer region at 0.6 V. Using the average charge density value of 210 µC cm^{-2} for one complete monolayer of adsorbed H on Pt.[63-65], it is possible to calculate respective ESCAs. By neglecting the H-absorption of Pd and assuming its H-adsorption charge density value of 210 µC cm^{-2}, equal to that of Pt,[41-43,63] the resulting ECSAs for Pd are generally overestimated.

The ESCAs A_O were determined by integrating the reduction peak resulting from the desorption of surface-oxides species subtracting the preceding capacitive currents from the bilayer region

at 1 V. The integrated charges can then be correlated to the ESCA: The charge values associated with the reduction of one monolayer of PdO and PtO are 424 µC cm^{-2} and 420 µC cm^{-2}, respectively.[63] Table 3 shows the entire evaluation of electrochemical data corresponding to surface normalization, normalized pcds and potential of recurring MOR at decreasing potential.

Table 3: Characteristic electrochemical values for the investigated Pd/Pt-NT samples. From left to right: atomic Pd/Pt-ratio, A_H: H-normalized calculated electrochemical surface area (ESCA), A_O: O-normalized calculated ESCA, pcd_H: peak current density (H-normalized), pcd_O: peak current density (O-normalized), E_r: potential of recurring MOR at decreasing potential

Pd_xPt_{100-x} [at%]	A_H [cm^2]	A_O [cm^2]	pcd_H [mA/cm^2]	pcd_O [mA/cm^2]	E_r [V]
Pd_0Pt_{100}	27.15	23.39	0.162	0.108	0.87
$Pd_{20}Pt_{80}$	24.02	19.85	0.363	0.226	1.10
$Pd_{30}Pt_{70}$	32.13	31.79	0.325	0.153	0.97
$Pd_{50}Pt_{50}$	29.09	14.18	0.156	0.113	0.92
$Pd_{75}Pt_{25}$	67.27	45.16	0.101	0.019	0.57
$Pd_{80}Pt_{20}$	70.24	27.20	0.035	0.002	0.51
$Pd_{100}Pt_0$	128.00	41.86	0.009	0.001	0.48

Samples $Pd_{20}Pt_{80}$ and Pd_0Pt_{100} were indirectly CO-poisoned through potentiostatic application at 1 V in 0.1 M formic acid. Figure 9 shows the first cycle in 0.5 M H_2SO_4 for these two samples: Both samples show a CO-stripping peak in the forward curve indicating the surficial removal of poisoning CO-species. In this experiment the distinctness of the CO-stripping peaks is variable, because the indirect poisoning procedure cannot assure poisoning the entire active surface of the catalyst. However, a clear evidence for a better CO-stripping capability of the $Pd_{20}Pt_{80}$ sample is the shift of the respective peak towards lower values: from 500 mV for the pure Pt sample to 445 mV. This observation indicates the occurrence of synergistic effects between Pd and Pt regarding CO-stripping capability.

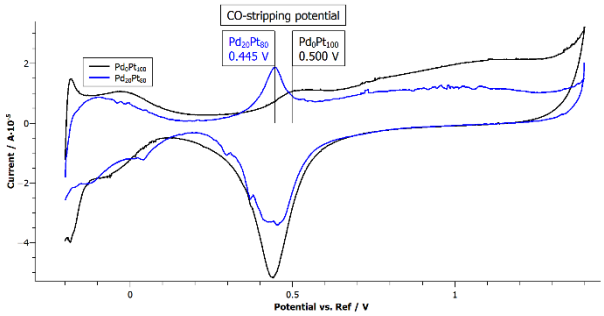

Figure 9: First cycle in 0.5 M H_2SO_4 after 1 h of indirect CO-poisoning for samples $Pd_{20}Pt_{80}$ and Pd_0Pt_{100}